TP53 mutations in endometrial cancer contribute to clinically-relevant radiation resistance and highlight the potential for biomarker-driven radiosensitization strategies.

Authors: Roberto Vargas, MD*[1,2]; Aaron Petty, MS[2]; Arda Durmaz, MS[2]; Kristi Lin-Rahardja, BAS[2]; Ofer Reizes, PhD[4]; Robert Debernardo, MD[1]; Jacob Scott MD, PhD*[2,3]

Affiliations:
1) Division of Gynecologic Oncology, Women's Health Institute, Cleveland Clinic
2) Department of Translational Hematology and Oncology Research, Lerner Research Insitute, Cleveland Clinic
3) Division of Radiation Oncology, Taussig Cancer Center, Cleveland Clinic
4) Center for Cardiovascular and Metabolic Sciences, Lerner Research Institute, Cleveland Clinic

Corresponding Authors:
Roberto Vargas, MD
Division of Gynecologic Oncology, Women's Health Institute
Department of Translational Hematology and Oncology Research
9500 Euclid Ave A-81
Cleveland, OH 44195
vargasr@ccf.org

Jacob Scott, MD, PhD
Department of Translational Hematology and Oncology Research
Lerner Research Institute
2111 E. 96th Street NE6
Cleveland, Ohio 44106
scottj10@ccf.org

Abstract:

Endometrial cancer (EC) is the most common type of gynecologic malignancy in the United States, with over 65,950 new cases expected in 2022. Approximately 80% of cancer-related mortalities can be attributed to high-grade EC. Despite our ability to identify different biologic clusters of EC, we have yet to understand the functional and therapeutic impact of the key genomic alterations associated with poor prognosis EC and exploit this knowledge for therapeutic benefit. Given this, we set out to determine if and how common TP53 alterations found in high-grade ECs impact radiotherapy response, and if manipulation of this signaling pathway could be utilized for therapeutic intervention. Our work demonstrates that p53 signaling plays a significant role in radiotherapy response for EC and that leveraging this genomic data may allow us to exploit this pathway as a viable therapeutic target.

Introduction:

Endometrial cancer (EC) is the most common gynecologic malignancy in the United States, with over 65,950 new cases expected in 2022.[1] Current trends outpace prior projections, with a 55% increase in incidence predicted from 2010 to 2030.[2] Endometrial cancer mortality rates now approaches that of ovarian cancer, the most lethal gynecologic malignancy, highlighting the need for increased investigative focus. As such, there has been a significant exploration attempting to elucidate the genomic underpinnings of EC [3–7] and the development of prognostic capabilities based on these findings.[8,9] Despite our ability to identify different biologic clusters of EC, we have yet to

understand the functional and therapeutic impact of the key genomic alterations associated with poor prognosis EC and exploit this knowledge for therapeutic benefit.

Approximately 80% of EC mortality can be attributed to high-grade tumors, as defined by histologic findings.[10] The majority of high-grade tumors also align with the "serous-like" biologic cluster, conferring a worse prognosis compared to other clusters.[3] The most common alterations identified within this cluster, and high-grade tumors, are *TP53* missense mutations and an increase in somatic copy-number alterations (sCNA).[3,7] While the direct relationship between sCNA and *TP53* mutations in EC has not been defined, loss or alteration of *TP53* has been previously shown to increase the probability of non-disjunction events leading to chromosomal instability in colon cancer cell lines.[11] These DNA repair events could provide the evolutionary link between both observed genomic alterations.[12–14]

TP53 alterations have also been previously associated with differential response to radiotherapy[15,16], but this finding has not been directly investigated in EC. Given that radiation therapy (RT) has remained the mainstay in adjuvant therapy over the last 3 decades, the identification of molecular subtypes that could benefit from (de)escalation will be paramount to improving outcomes.[7,17–19] Furthermore, the allelic frequency of *TP53* mutations has been demonstrated to negatively impact clinical outcomes in myelodysplastic disorders[15,20–23] and the development of sCNA alterations[14].

The fundamental molecular and biologic rationale driving discrepant clinical outcomes in EC is lacking. Given this, we set out to determine the association between *TP53* VAF and clinical outcomes in EC, as well as the direct therapeutic impact of *TP53*

alterations using cell lines. We also evaluated if pharmacologic manipulation of this signaling pathway, through inhibition of p53 degradation with MDM-2 inhibitors, is a viable therapeutic avenue. To accomplish these goals, we integrated clinical data from the TCGA study with high-throughput radiation phenotyping, intron-targeting CRISPR/Cas9 techniques, and dose-response assessments using cell lines.

Results:

***TP53* variant allelic frequency is associated with worse clinical outcomes in EC**

Using available data from comprehensive genomic profiling efforts in The Cancer Genome Atlas, we conducted survival analyses on patients with FIGO stage I-III EC. We found that the prevalence of *TP53* mutations is highly correlated with tumors having increased sCNA burden, but not exclusively limited to that group. **[Fig 1a]** Patients who received radiotherapy were more likely to have higher-grade tumors and increased tumor mutational burden, compared to those who do not receive radiotherapy. **[Table S1a]** On univariate analysis, histologic grade, FIGO stage, SCNA, and *TP53* status were all associated with worse progression-free survival (PFS). **[Table S1b]** On multivariable analysis only the FIGO stage was associated with a worse prognosis, supporting the notion that *TP53* mutations and copy-number high status often co-exist in EC. **[Table S1c].**

Patients with *TP53* alterations had a significantly worse PFS (HR 1.9, 95% CI 1.0 - 3.7, log-rank p = 0.046) compared to patients with wild-type *TP53,* despite treatment with RT**. [Fig 1b]** When stratified by *TP53* variant allelic frequency (VAF), only patients with a high VAF had a significantly worse PFS after RT treatment, compared to low VAF

Figure 1. TP53 Variant Allelic Frequency Is Clinically Relevant in Endometrial Cancer

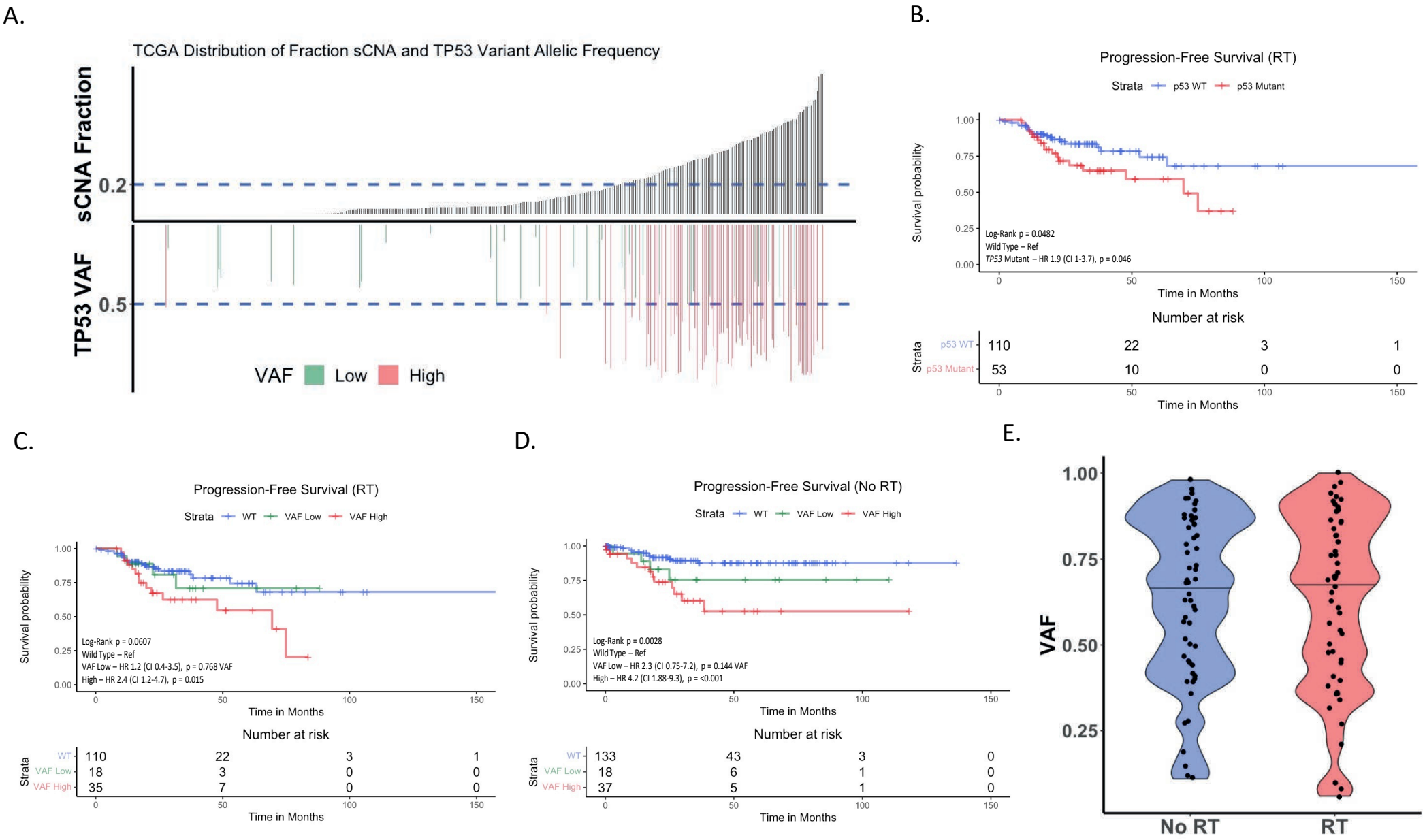

Figure 1. TP53 Variant Allelic Frequency Is Clinically Relevant in Endometrial Cancer - A) This plot represents available EC patients in cbioportal with somatic copy number alteration (sCNA) burden and TP53 data available. The dashed line at 0.2 defines the cutoff for copy-number high used in TCGA. As noted, the frequency of TP53 mutations increases with increasing sCNA. While the majority of TP53 mutations have a high variant allelic frequency (VAF), there remain patients with <50% allelic frequency throughout the entire population. **B-D)** Kaplan-Meier plots and Cox-regression for progression free survival (PFS) stratified by TP53 status **(B)** and TP53 VAF **(C-D)**. As noted in subfigure B, patients with TP53 mutation had worse PFS compared to wild-type patients when treated with RT. When stratified by VAF (**C),** patients with a high VAF had a worse PFS compared to low VAF and wild-type patients. We observed the same in non-RT patients **(D)**, albeit the difference in risk of progression based on hazard ratio was more notable between low VAF and wild-type. **E)** Violin plot representing the overall distribution of TP53 VAF in both treatment groups, highlighting that current treatment patterns do not take VAF into consideration.

TP53 (HR 2.01, 95% CI 0.66 - 6.1) and wild-type *TP53* tumors (HR 2.4, 95% CI 1.2 – 4.7, log-rank p = 0.015). In the face of radiotherapy, low VAF patients responded most like WT patients. **[Fig Ic, Fig S1].** The differential outcome based on VAF was also observed with patients who did not receive RT, highlighting the established prognostic value of p53 mutations. Yet the trend in the hazard ratios in low VAF patients suggests that *TP53* allelic frequency may also have predictive value in regards to radiation response **[Fig 1d, Fig S1].**

While the majority of patients in the "serous-like" cluster will have a high-VAF (>0.5) *TP53* mutation, 15% of these high-risk patients retain a low VAF **[Table 1].** This sub-set of patients belonging to "poor-prognosis" genomic and histologic groups will have clinical outcomes similar to low-grade/wild-type tumors. Notably, the median VAF was not significantly different between the no RT and RT groups **[Fig 1e]**, highlighting that despite the established clinical difference in outcomes the administration of RT is not currently tailored based on *TP53* status. Understanding the molecular and therapeutic impact, as well as the predictive capabilities of VAF *TP53* in EC, may allow treatment personalization.

TP53 status impacts radiotherapy response in EC cell lines

Using a validated high-throughput radiation profiling platform[24], we correlated the effect of TP53 status on gamma-radiation response on a panel of EC cell lines. Endometrial cancer cell lines with altered *TP53* status were more likely to have higher radiation resistance/area under the curve (AUC) (LR 11.12, p = 0.004). When stratified

Table 1. Stratification of *TP53* mutant patients based on VAF highlights other associated genomic markers.

Characteristic	P53 Variant Allele Frequency		
	High, N = 72[1]	**Low**, N = 36[1]	**p-value**[2]
Age at Diagnosis	69.00 (8.88)	64.00 (10.64)	0.057
Total Mutation Count	60.00 (42.28)	176.50 (2,837.31)	<0.001
Fraction Genome Altered	0.43 (0.18)	0.15 (0.19)	<0.001
TCGA Cluster			<0.001
UCEC_CN_HIGH	67 / 69 (97%)	16 / 36 (44%)	
UCEC_CN_LOW	1 / 69 (1.4%)	4 / 36 (11%)	
UCEC_MSI	1 / 69 (1.4%)	13 / 36 (36%)	
UCEC_POLE	0 / 69 (0%)	3 / 36 (8.3%)	
FIGO Stage			>0.9
I	37 / 72 (51%)	20 / 36 (56%)	
II	10 / 72 (14%)	4 / 36 (11%)	
III	25 / 72 (35%)	12 / 36 (33%)	
Histologic Grade			0.4
1	0 / 72 (0%)	1 / 36 (2.8%)	
2	7 / 72 (9.7%)	4 / 36 (11%)	
3	65 / 72 (90%)	31 / 36 (86%)	
Radiation Therapy	35 / 72 (49%)	18 / 36 (50%)	0.9

[1] Median (SD); n / N (%)

[2] Wilcoxon rank sum test; Fisher's exact test; Pearson's Chi-squared test

Table 1. Stratification of TP53 mutant patients based on VAF highlights other associated genomic markers. Demographics table of patients with TP53 alterations stratified by their variant allelic frequency. High is defined as >50% and low is defined as <50%. As noted, patients with a low VAF were more likely to have higher mutational counts, lower copy-number alterations, and less likely to be classified into the "serous-like" (UCEC_CN-HIGH) TCGA cluster. When taken as an entire group, the "serous-like" cluster had 105 patients, with 16 (15%) falling into the low VAF classification. No differences in clinical stage, histologic grade, or receipt of adjuvant radiation (RT) therapy was noted.

by allelic frequency, those with a VAF >0.5 (high VAF) were also more likely to be associated with radiation resistance/higher AUC (LR 9.42, p=0.009). **[Fig 2a]** Using an intron-targeting CRISPR/Cas9 system, we then conducted a complementation experiment using a subset of EC cell lines. A statistically significant increase in the AUC (representative of radiation resistance) was observed when JHUEM-1 and JHUEM-2 cell lines (both wild-type *TP53)* underwent CRISPR/Cas9 knock-out (KO) of *TP53*. **[Fig 2b]** As noted on Western blotting, signaling through the p53/p21 pathway was disrupted with KO **[Fig 2c].** No discernible change in the AUC for radiation response was observed in CRISPR/Cas9 *TP53* knockouts in the Hec1A, Hec1B, and MFE-319 cell lines, all of which contained high-VAF GOF/DN *TP53* alterations**. [Figure S2]**

Complementation with a low-expression (PGK) vector containing wild-type *TP53* re-established p53/p21 signaling **[Fig 2d]** and radiation sensitivity **[Fig 2e]** in JHUEM-1/JHUEM-2 that had parental wild-type alleles previously knocked out. Complementation of our copy-number high/*TP53*-KO constructs (Hec1A, Hec1B, and MFE319) with a wild-type *TP53* vector did not reintroduce significant radiation sensitivity. It is plausible that the evolutionary trajectories of these *TP53* mutant cell lines have allowed for the amplification of other genomic drivers of resistance aside from the direct impacts of p53/p21 signaling.

Gain-of-function/dominant-negative *TP53* mutations negatively impact radiotherapy response

Employing the same *TP53-KO* constructs we subsequently explored the impact of five hotspot *TP53* alterations (R248Q, R248W, R273C, R273H, Y220C) representing the

Figure 2. *TP53* Status and VAF are Associated with Radiation Resistance in EC Cell Lines

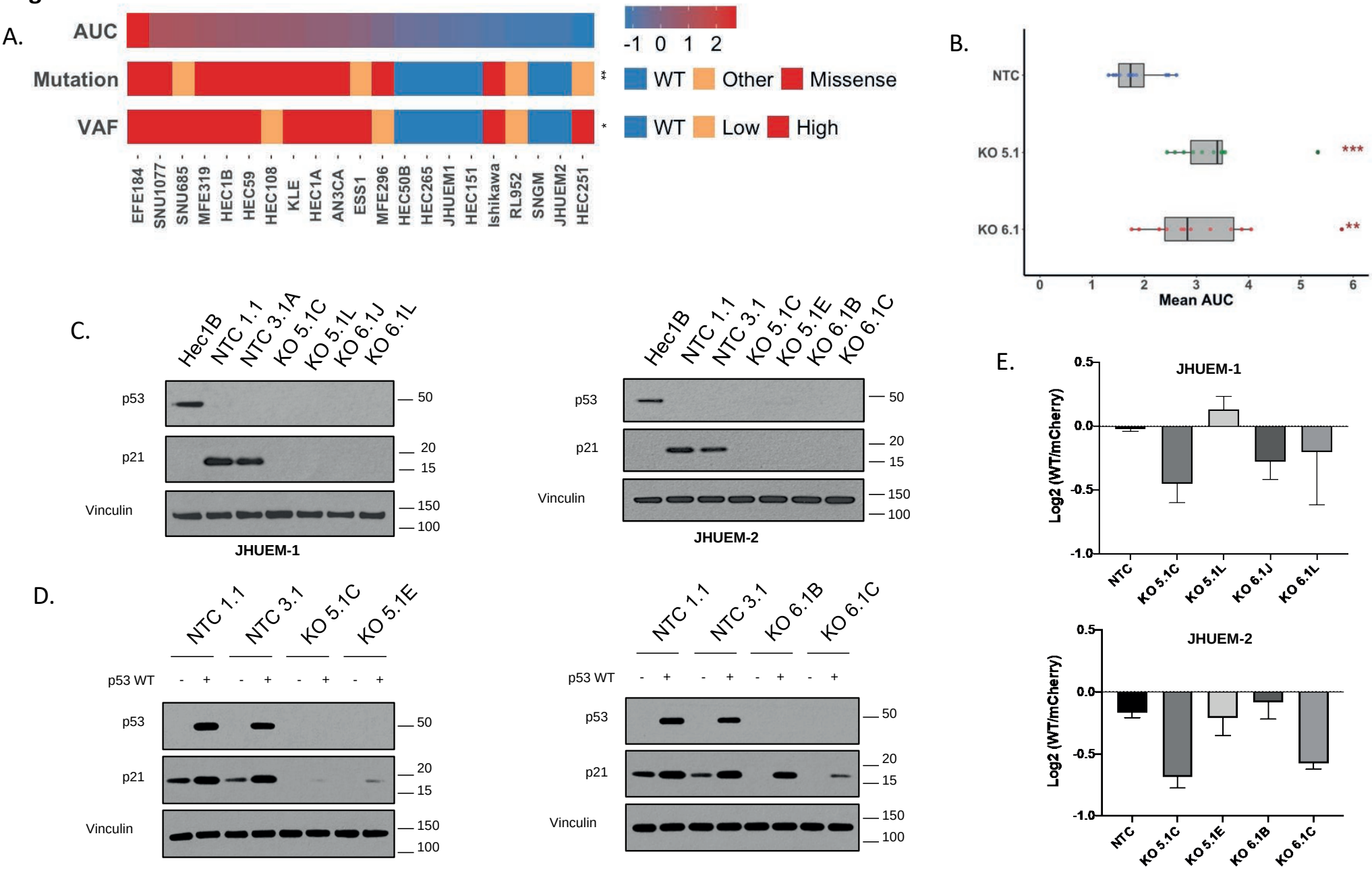

Figure 2. *TP53* Status and AF are Associated with Radiation Resistance in EC Cell Lines – A) Heat-map depicting 21 EC cell lines organized by decreasing radiation resistance (left to right) as quantified by area under the curve (AUC). The cell lines' TP53 mutational status and VAF are depicted in the bars below, denoting the significant associations between AUC and *TP53* mutation status ($p = 0.004$) or VAF ($p = 0.01$), respectively. A linear regression model was fitted to assess for the correlation between mutation and AUC (Likelihood Ratio = 11.12 and P= 0.0038) as well as VAF and AUC (Likelihood Ratio = 9.42 and P= 0.009). **B)** Box-whisker plot depicting the increase in radiation AUC noted with two different CRISPR/Cas9 guide-RNA (gRNA) sequences for TP53 compared to the non-targeting control (NTC). Kruskal-Wallis test with Dunn's Multiple Comparisons Test was performed with $p< 0.001$ for NTC vs KO 5.1, $p = 0.0016$ for NTC vs KO 6.1. **C)** Western-blot analysis of two monoclonal isolates from each gRNA and NTC reveals loss of p21 signaling with knock-out of TP53. Hec1B is our positive control for p53. **D-E)** Complementation with wild-type TP53 re-establishes p21 signaling and radiation sensitivity in knock-out clones. For subfigure E and JHUEM2 ,one- way ANOVA test with Dunnett's Multiple Comparisons test was performed with $p = 0.0051$ for KO 5.1C vs NTC, $p = 0.0199$ for KO 6.1C vs NTC.

top 3 amino acid residues altered in EC. First, the effect of each mutation on p53/p21 signaling and radiation phenotype was assessed. We noted that the introduction of these hotspots into a *TP53*-KO (p53 null) cell line did not re-establish p53/p21 signaling **[Fig 3a, Fig S3]** or change radiation resistance**.** When the mutations were co-expressed with wild-type *TP53* present in our non-targeting controls a dominant-negative effect was confirmed **(Fig 3b).** The 5 hotspot variants led to an increase in radiation resistance, despite the presence of two parental wild-type alleles. Concurrently, an abrogation of the p53/p21 signaling was observed **(Fig 3c),** supporting the notion that p53 signaling through the p21 pathway is negatively affected by these variants and contributes to resistance.

To assess for potential off-target effects of dominant-negative variants, we treated our JHUEM2 non-targeting controls (NTC) with parental wild-type alleles and the JHUEM2 (NTC + R273C) constructs with 2Gy of gamma radiation. RNA was extracted 24 hours later and differential gene expression analysis was performed. Hallmark pathways that were significantly altered in the *R273C* co-expressing cell lines (1.1RC and 3.1RC) included apoptosis and tumor necrosis-alpha gene sets, mainly driven by down-regulation of *CDKN1A, BTG2, CCND1, GADD45B, NINJ1, IER2, and FAS.* **[Fig 3d, Table S2].**

MDM-2 inhibition sensitizes EC cell lines by increasing wild-type signaling

MDM-2 inhibitors are a class of small molecules that inhibit the E3-ubiquitin ligase responsible for the degradation of p53. MDM-2 inhibitors have been tested in other solid malignancies, but their role in the treatment of EC has not been assessed. Given the

Figure 3. Gain-of-Function/Dominant-Negative Alleles of *TP53* Impact p21 Signaling, Radiation Response and apoptosis

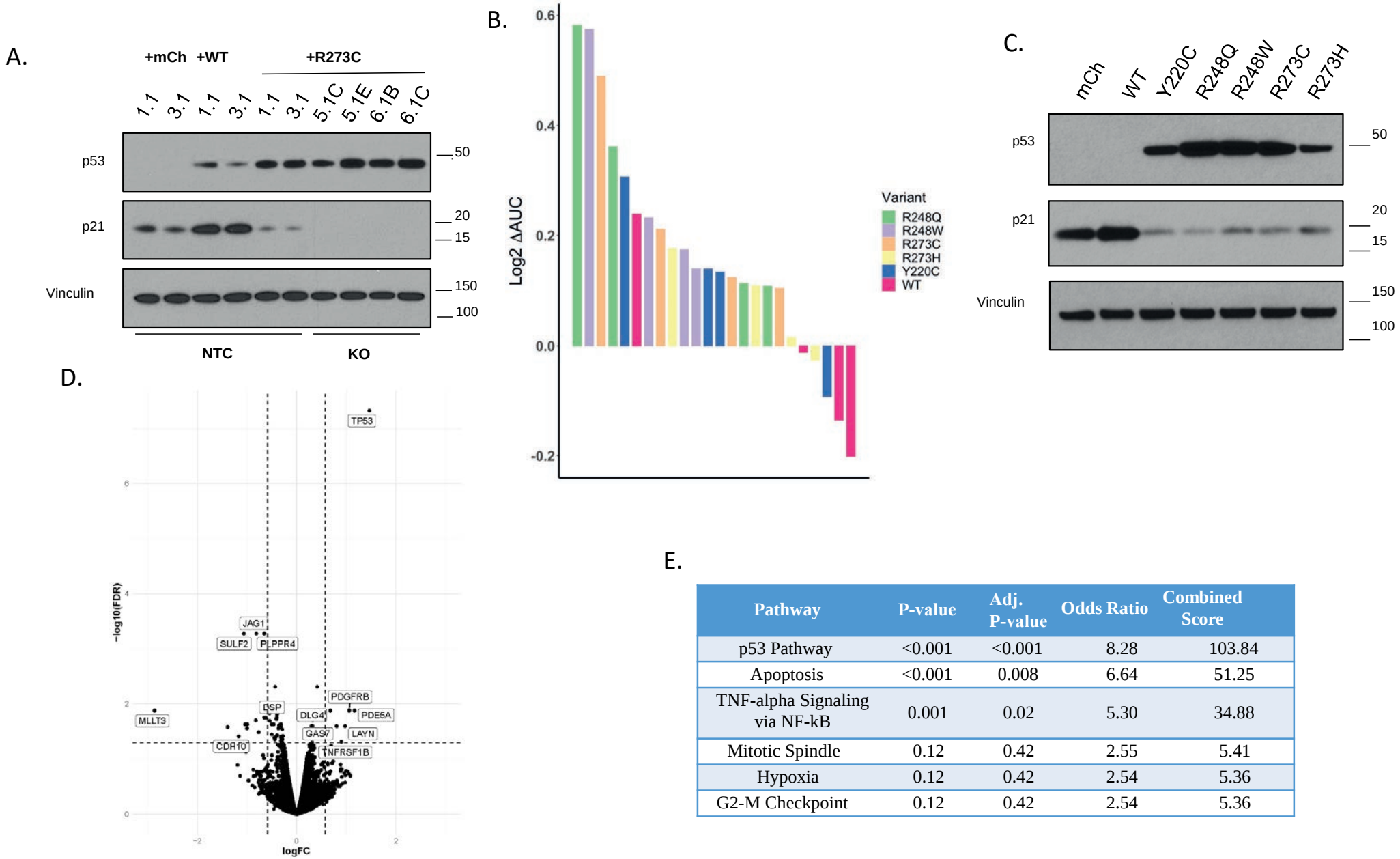

Pathway	P-value	Adj. P-value	Odds Ratio	Combined Score
p53 Pathway	<0.001	<0.001	8.28	103.84
Apoptosis	<0.001	0.008	6.64	51.25
TNF-alpha Signaling via NF-kB	0.001	0.02	5.30	34.88
Mitotic Spindle	0.12	0.42	2.55	5.41
Hypoxia	0.12	0.42	2.54	5.36
G2-M Checkpoint	0.12	0.42	2.54	5.36

Figure 3. Gain-of-Function/Dominant-Negative Alleles of TP53 Impact p21 Signaling, Radiation Response, and Apoptotic Pathways – **A)** Western-blot analysis of JHUEM-2 non-targeting control [NTC] isolates (1.1 and 3.1) with the addition of mcherry (control), wild-type TP53 (over-expression), and the addition of the R273C allele (co-expression with wild-type). A decrease in p21 signaling after introduction of the R273C allele is noted in the NTC isolated, despite parental/wild-type TP53 alleles. In the knockout isolates (5.1C/E and 6.1B/C) there is no p21 signaling observed with the mutant allele alone. **B)** Waterfall plot depicting the overall effect on AUC after introduction of a variant allele (or wild-type) across 4 different mono-clonal NTC isolates. As noted, introduction of variant alleles led to an increase in radiation resistance from baseline despite the presence of a wild-type allele. **C)** Western-blot analysis demonstrating decrease in p21 signaling with each analyzed GOF/DN TP53 variant. **D)** Volcano plot analysis of an the NTC isolates with R273C co-expression, compared to the NTC alone (wild-type) 24hr after 2Gy irradiation. An increase in the expression of TP53 in our wt/R273C isolate confirms increased expression of p53, with a decrease in the expression of genes associated with apoptosis and TNF-alpha signaling **(E).**

significance of the p53/p21 signaling pathway in EC cell lines, we explored the concept of MDM-2 inhibition as a cytotoxic and/or radio-sensitizing strategy. Nutlin-3 is a first-generation MDM-2 inhibitor, while AMG-232 is a potent MDM-2 inhibitor undergoing clinical trial testing in soft-tissue sarcomas. Using three parental cell lines to replicate a wild-type (JHUEM2), low-VAF (Hec 108), and high-VAF (Hec1B) endometrial malignancy, we performed cell viability experiments using both Nutlin-3 and AMG-232. A differential effect on cell viability was observed depending on the presence of wild-type *TP53,* co-expression of wild-type/variant, or expression of only the GOF/DN allele. Only the cell lines with a wild-type allele present (JHUEM2 and Hec108) have decreased cell viability **(Fig 4a)** and downstream p21 activation **(Fig 4b)** in response to treatment with Nutlin-3. Treatment of three parental EC cell lines with AMG-232 confirmed the more potent effect on cell viability **(Fig 4c)** and induction of p21 **(Fig 4d)** than with the first-generation MDM-2 inhibitor. Hec1B, with high-VAF *TP53,* is resistant to treatment with both MDM-2 inhibitors, consistent with prior studies.[25] To assess clinical relevance, we queried the TCGA cohort for MDM2 expression in EC. We noted a negative correlation between MDM2 expression and *TP53* status; patients with wild-type or low-VAF *TP53* mutant EC retained some expression of MDM2. **[Fig 4e].**

When the same cell lines are treated with Nutlin-3 and exposed to a range of doses of gamma radiation, Nutlin-3 treatment results in a synergistic effect in JHUEM2 and an additive effect in Hec 108 **[Fig 5a,c].** AMG-232 showed a synergistic effect in both the JHUEM2 and Hec108 *TP53*-mutant cell lines. **[Fig 5b,c, S5]** These findings deepen our understanding of the relationship between MDM-2 inhibition and *TP53*, allowing for potential therapeutic development and novel applications in EC.

Figure 4. MDM2 Inhibition with Nutlin-3 and AMG-232 as a Cytotoxic Strategy

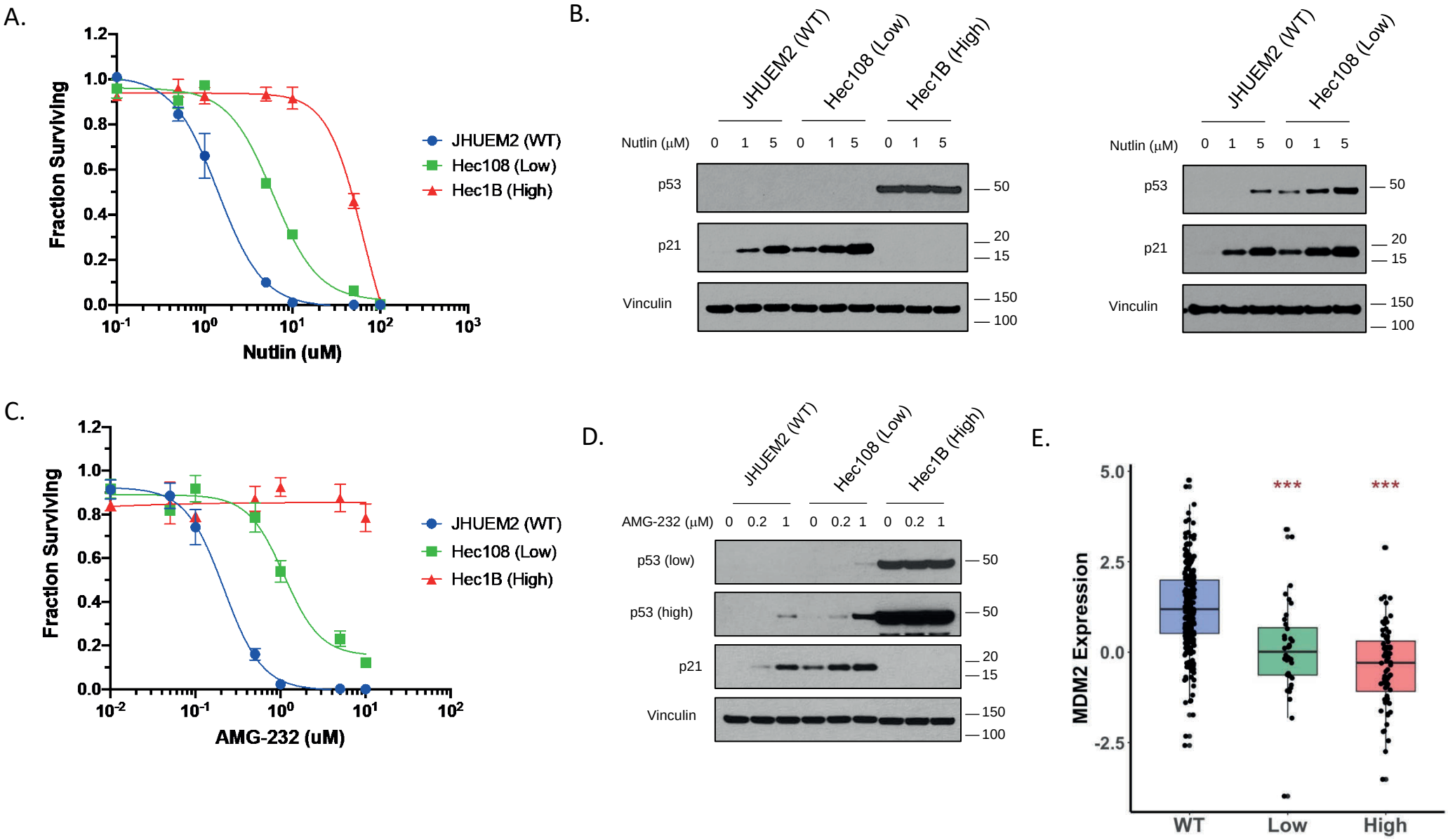

Figure 4. MDM2 Inhibition with Nutlin-3 and AMG-232 as a Cytotoxic Strategy. A, C) – Drug response curve of EC cell lines representing three different VAF populations – JHUEM2 (wild-type), Hec108 (low-VAF), and Hec1B (high-VAF). Nutlin-3 **(A)** and AMG-232 **(C)** both demonstrate significant effects on cell viability in JHUEM2 and Hec 108. Hec1B was resistant to treatment with either drug. **B, D)** Western-blot analysis of all three cell lines demonstrate an increase in p53/p21 with increasing concentrations of either drug. **E)** Box-whisker plot of MDM2 expression across TCGA patients demonstrate that MDM2 expression decreases with increasing VAF, but there remains a significant portion of low-VAF patients with mRNA expression that could be targeted via Nutlin-3/AMG-232. For subfigure E, one-way ANOVA with Tukey's Multiple Comparisons Test was conducted to analyze relative expression compared to the WT group. $p < 0.001$ for Low vs WT ; $p < 0.001$ for High vs WT.

Figure 5. MDM2 Inhibition Is Synergistic with Radiotherapy in EC with Wild-Type *TP53*

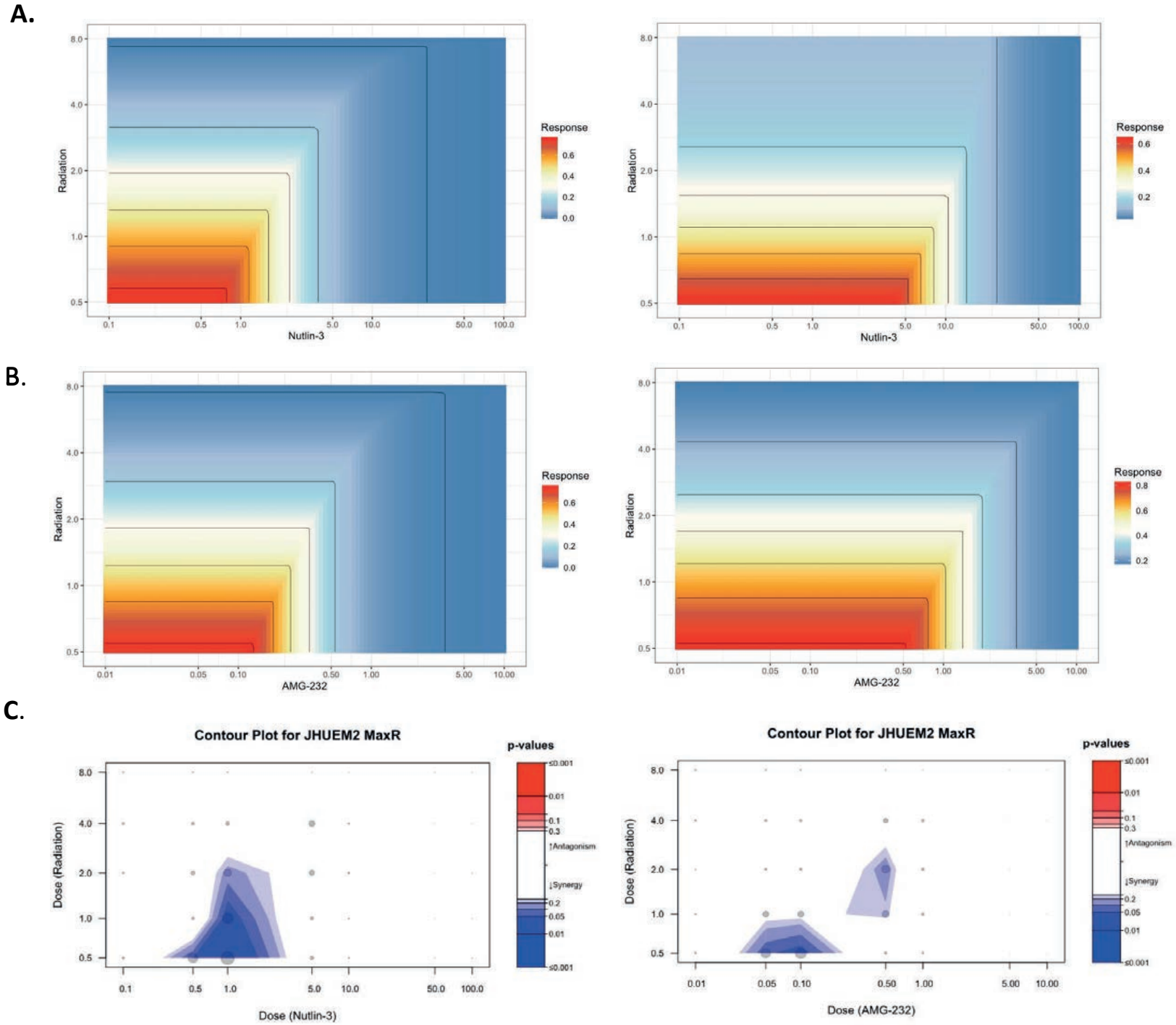

Figure 5. MDM2 Inhibition Is Synergistic (or Additive) with Radiotherapy Dependent on TP53 Status – A-B) Isobolograms for Nutlin-3 **(A)** and AMG-232 **(B)** in two EC cell lines - JHUEM2 (left) and Hec108 (right) - treated with gamma irradiation. As depicted, increasing drug dosage is the x-axis and increasing radiation dose is the y-axis. A robust effect on Nutlin-3 and AMG-232 is achieved at low drug concentrations and low RT doses for both the wild-type (JHUEM2) and low VAF (Hec108) cell line. **C)** Contour plots quantitatively demonstrate the synergistic effect of Nutlin-3 in JHUEM2 (left), as well as with AMG-232 in JHUEM2 (right) and Hec108(supp Fig 5). The remaining interactions were classified as additive. Synergy was quantified by comparing actual values to those predicted by fitting the Highest Single Agent (HSA) model to the data.

Discussion:

Our integrative analysis incorporating a clinically annotated dataset, high-throughput radiation phenotyping, complementation experiments using CRISPR/Cas9, and pharmacologic targeting, provides a full-spectrum fundamental biologic rationale behind the disparate clinical outcomes in EC. While the prognostic value of *TP53* status in EC has previously been observed in clinical trials, the precise therapeutic impact remained poorly understood. Using the aforementioned strategies, we are the first to demonstrate that allelic frequency of *TP53* alterations is prognostic, and possibly predictive, in EC. We also confirm the oncogenic gain-of-function impact, by way of radiation resistance, with dominant-negative variants. Lastly, our study demonstrates that not all *TP53* mutant cell lines are resistant to MDM-2 inhibition- and the degree of resistance depends on the variation in the amount of functional wild-type p53.

We first compared outcomes in EC patients treated with radiotherapy, stratified by the presence of *TP53* alterations and their allelic frequencies. As with most malignancies, alterations in this pathway confer a poor prognosis, yet there is emerging data that supports the consideration of allelic frequency in clinical decision-making. In MDS/AML, patients with high-VAF *TP53* mutations have been shown to have worse overall survival. Conversely, patients with low-VAF *TP53* alterations had clinical outcomes similar to those of patients with wild-type *TP53.* These observations could impact treatment considerations, such as bone-marrow transplantation. Within our EC data, the subgroup of patients with low-VAF *TP53* alterations had outcomes after radiotherapy that were similar to those of patients with wild-type p53. Taken together, this information supports that an intact p53 signaling pathway may remain functionally relevant in a significant

group of EC patients, including the 15% who would have previously been deemed of poor prognosis and receive (unnecessary) escalated therapy.

Given that the majority (80%) of EC have WT *TP53,* we first focused on wild-type/low-grade cell lines to demonstrate that the loss of this key oncogene resulted in the development of radiation resistance. Subsequently, we noted that restoration of a wild-type allele re-established p53/p21 signaling and restored a small degree of radiation sensitivity. We attribute the low expression of wild-type *TP53* by the PGK promoter in our vector to explain the lack of a complete phenotype restoration. Using the same complementation approach also allowed for the assessment of common hotspot mutations (Y220C, R273C/H, and R248Q/W) and their functional impact. While the mutations themselves provided a GOF phenotype by conferring radioresistance, they also exhibited a dominant-negative effect on wild-type signaling. Despite a low-expression vector, the introduction of all 5 missense mutations suppressed p21 signaling established by the two parental wild-type *TP53* alleles. Furthermore, we demonstrate that the GOF/dominant-negative alleles also conferred a radio-resistant phenotype.

Gene-expression changes observed after treatment with 2Gy of radiation support the notion that these common mutations may be targeting other pathways relevant to radiation response. Our pathway analysis shows genes associated with apoptotic pathways and tumor necrosis factor-alpha (TNFα) signaling via NF-κB are down-regulated in the presence of the R273C allele and irradiation. Pal *et al*. previously demonstrated that TNFα influences radiation-mediated DNA damage, with decreased TNFα leading to reduced double-stranded breaks in lung cancer cell lines.[26] Additionally, the same authors found that serum TNFα expression positively correlated with clinical

outcomes after radiotherapy. The degree of TNFα induction after irradiation has also been shown to predict clinical radiotherapy response in multiple solid tumors.[27] While TNFα/NF-κB signaling has been shown to have both pro-apoptotic and anti-apoptotic properties based on cell/tumor lineage[28], in our *TP53*-altered (R273C) EC cell line we saw a decrease in the expression of genes associated with TNFα/ NF-κB signaling, as well as other apoptosis-related genes when treated with radiation. Prior studies in prostate cancer cell lines have also noted a decrease in NF-κB is associated with anti-apoptotic effects after radiation.[29,30] Crosstalk between p53 and TNFα/NF-κB through non-canonical pathways may be contributing to cell survival after irradiation.[31]

We additionally performed pharmacologic exploitation of intact p53 signaling using MDM-2 inhibitors. Both Nutlin-3 and AMG-232 provided increased p53/p21 signaling and conferred a synergistic effect on parental cells with wild-type *TP53,* particularly at low doses of radiation and MDM2 inhibitors. Given that the majority of EC (80%) retain wild-type TP53, this foundation could lead to genomic-based radio-sensitizing schemes for low-grade EC. Furthermore, we noted that even in the presence of a GOF mutation, MDM2 inhibitors provide at least an additive effect when given in combination with radiotherapy. This further broadens the potential application of MDM-2 inhibition in personalized radiation therapy. Further *in-vivo* experimentation is needed to validate these translational findings.

In summary, our study provides a biologic rationale behind the observed clinical outcomes of many gynecologic oncology trials - *TP53* alterations confer resistance to radiotherapy in EC. Furthermore, we also demonstrate that dominant-negative alleles impact radiation response via abrogation of the classical p53/p21 pathway and may also

interfere with TNF-alpha response. Lastly, we provide support for the investigation of MDM-2 inhibitors as novel radio-sensitizing agents in wild-type and low-VAF *TP53*-mutant EC.

Methods:

Survival Analysis. Clinical data was obtained from cbioportal.org and curated from the uterine cancer TCGA Firehose Legacy, Nature 2013, and PanCancer Atlas datasets.[32,33] All patient identifiers were matched to collate clinical and genomic markers for analysis. Duplicate samples were removed. Only patients with tumor genomic data (*TP53* status, allelic frequency, tumor mutational burden, fraction genome altered, biologic cluster) and clinical data (age at diagnosis, race, FIGO stage, tumor histologic grade, adjuvant radiotherapy, progression-free survival) were included in the final dataset for analysis. Patients with multiple *TP53* mutations or stage IV disease were excluded, as well as those receiving adjuvant chemotherapy. Kaplan-Meier and Cox proportional hazards analyses were performed to assess for impact on progression-free survival (PFS). Multivariable analyses were performed on clinical/genomic variables with significance on univariate analysis.

Cell culture. JHUEM1, JHUEM2, and Hec108, cells were grown in DMEM-F12 media containing 15 mM HEPES and 2.5 mM L-Glutamine (Thermo Fisher, MA) and supplemented with 10% FBS, 100 U/mL Penicillin, 100 µg/mL of Streptomycin. Hec1A, Hec1B, MFE319, and HEK293T cell lines were grown in DMEM media containing 4.5 g/L Glucose, 1 mM Sodium Pyruvate, 4 mM L-Glutamine (Thermo Fisher, MA) supplemented

with 10% FBS, 100 U/mL Penicillin, 100 µg/mL of Streptomycin. All cultures were maintained at 37 °C in a humidified 5% CO_2 atmosphere. All cell lines were verified by human short-terminal repeat (STR) analysis (Labcorp, NC) and tested to ensure the absence of *Mycoplasma* via qPCR.

Lentivirus production and infection. Lentivirus containing all mentioned plasmids was generated by transfecting HEK293T cells with the appropriate plasmid along with the psPAX2 (Addgene; Plasmid #12260) and pMD2.G (Addgene; Plasmid #12259) plasmids in a 5:4:1 ratio. Around 18 hours following transfection media was changed, followed by the collection and purification of lentiviral-containing supernatants over the next two days. Centrifugation and passage through a 40 uM filter were used for purification. Cell lines were infected with these viruses at an MOI > 0.8 in media supplemented with 5 ug/ml Polybrene.

Exon-intron junctional CRISPR. sgRNAs that target the exon 5-intron (5.1) and exon 6-intron (6.1) junctions of *TP53* were designed with the Synthego CRISPR web design tool (https://www.synthego.com/products/bioinformatics/crispr-design-tool/). Non-targeting control (NTC) sgRNAs were also designed. For each sgRNA, two complementary oligos with BsmBI digestion overhang sequences were designed. Sequences of sgRNAs can be found in **Supplementary Table 3.** plentiCRISPRv2-Blast plasmid (Addgene: Plasmid #83480), which contains the Cas9 coding sequence and a cloning site for sgRNA, was digested with BsmBI, followed by annealing of sgRNAs and ligation into the pLentiCRISPRv2-Blast plasmid as in the Zhang Lab protocol given at http://www.genome-engineering.org/gecko, as well as on the website for the original

pLentiCRISPRv2 plasmid (Addgene #52961).[34,35] Plasmids were transformed into NEB Stable bacteria (New England Biolabs, MA) and colonies were screened for sgRNA inserts by Sanger sequencing of the ligation site. After virus infection, cells were selected and maintained in the presence of 5 µg/mL blasticidin (Thermo Fisher, MA). Monoclonal cells were isolated from a polyclonal pool of transduced stable cells using the limiting dilution assay. Protein lysates were obtained from each clone and *TP53* KO was confirmed by Western Blot.

Variant-expressing plasmid generation. Variant-expressing lentiviral plasmids were generated by utilizing PCR-based site-directed mutagenesis, followed by bacterial recombination and transformation. First, 5' and 3' fragments containing incorporated mutated gene ORF sequences were amplified by PCR from the pDONR223-TP53 WT plasmid (Addgene; Plasmid #82754). In this case, the 5' and 3' flanking PCR primers were located at the attL1 and attL2 sites, with the internal primers containing incorporated mutated sequences. Sequences of PCR primers can be found in **Supplementary Table 4.** Fragments were then transferred to the destination vector pLEX306 (Addgene; Plasmid #49391) by LR reaction with LR Clonase II enzyme (Invitrogen, CA), followed by transformation into competent cells. The overlapping fragment overhangs at the mutation site were repaired by endogenous bacterial repair. Inserted sequences and incorporated mutation were verified by restriction digestion with BsrGI and Sanger sequencing of ORF, respectively.

Complementation. Wild type and variant containing ORFs of *TP53* were cloned into pLEX306 and integrated into the respective CRISPR KO or non-target control (NTC) cell

lines. After virus infection, cells were selected and maintained in the presence of 1 μg/mL puromycin.

Antibodies and reagents. Anti-p53 (#9282, 1:3000), anti-p21 Waf1/Cip1 (clone 12D1, #2947, 1:3000), anti-Vinculin (clone E1E9V, #13901, 1:5000) were from Cell Signaling Technology. Goat anti-rabbit antibody linked to horseradish peroxidase (HRP) was used as the secondary antibody (Santa Cruz Biotechnology, CA).

Western blot analysis. Cells were pretreated with 10 uM Nutlin-3 in 0.1% DMSO for 18 hours to enhance the protein signal to a detectable level for comparison. Cells for dose-response analyses were treated with an appropriate dose of 0.05% DMSO. Whole-cell lysates were prepared using M-PER lysis buffer (Thermo Fisher, MA) and clarified by centrifugation. Proteins were separated by SDS–PAGE on 4-12% Bis-Tris gradient gels (Thermo Fisher, MA) and transferred onto 0.2 μM nitrocellulose membranes (Bio-Rad, CA). Membranes were blocked and incubated in primary antibody for 2 hours at room temperature, followed by washing and incubation for 1h with secondary antibody. Blots were developed with the ECL Plus chemiluminescence system (Amersham/GE Healthcare, UK).

High-content radiation assay. Cells were plated using a Multidrop Combi liquid handler (Thermo Fisher, MA) at multiple cell densities in white 96-well plates (Corning, NY) for each cell line. Cells were plated in 6 replicate wells for each cell density in triplicate. Plates were irradiated and at 9 days post-irradiation, media were aspirated and 50 μL CellTiter-Glo® reagent (50% solution in PBS) (Promega, WI) was added to each well. Relative luminescence units (RLU), proportional to the amount of ATP present, were

measured using a Synergy H1 (Biotek, IL) luminescence plate reader. The luminescence signal was plotted as a function of cell density and a cell density within the linear range for luminescence was selected to generate integral survival for each cell line.[24] Cells were treated with γ-radiation delivered at 0.92 Gy/min with a ^{137}Cs source using the Mark 1 Irradiator (Shepherd and Associates, CA). The area under the curve (AUC) was estimated using a trapezoidal approximation in GraphPad Prism software (Version 8.4.3, GraphPad, CA). Radiation doses of 0, 2, 4, 6, and 8 Gy were given and the fraction surviving was determined by normalizing each RLU value to the 0 Gy value. These data were then used to generate an AUC value for each cell line.

Drug dose-response assays. For drug dose-response experiments, cells were plated as given above and treated with either 0.5% DMSO (Control), or 7 different doses of the drug in 0.5% DMSO. For Nutlin-3, doses of 0.1, 0.5, 1, 5, 10, 50, 100 uM were used and 0.01, 0.05, 0.1, 0.5, 1, 5, 10 nM for AMG-232. Cells were treated for 24 hours, followed by replacement with drug-free media and incubation for 9 days. Cells were then lysed with CellTiter-Glo reagent and RLU values were obtained as given above. Fraction surviving was determined by normalizing each RLU value to either the 0 Gy value, or the maximum value, whichever was greater. Four-parameter sigmoid curves were fitted to the dose-response data and IC50 values were determined using GraphPad Prism software (Version 8.4.3, GraphPad, CA).

Drug radiosensitization assays. For drug radiosensitization experiments, cells were plated and treated with drug doses as given above. Following replacement with drug-free media, radiation doses of 0, 0.5, 1, 2, 4, and 8 Gy were given, followed by incubation

for 9 days. For JHUEM2 and Hec108, cells in plates receiving 2, 4, and 8 Gy of radiation were plated at twice the density to allow accurate RLU signal detection and comparisons. Fraction surviving was determined by normalizing each RLU value to the Untreated (0 uM, 0 Gy) value. Fraction surviving values at 2, 4, and 8 Gy were halved to correct for higher plating density. The mean values for three replicates were taken and all were divided by the maximum signal. These data were used to perform synergy analysis. Briefly, the Highest Single Agent (HSA) additivity model was used to generate predicted additive response curves for the JHUEM2 and Hec108 data. The Loewe additivity model was used for Hec1B, as the data did not meet the requirements for HSA. The actual data was then compared and synergy scores generated based on the deviation of each point from the model.

RNA Isolation and RNA Seq. For RNA isolation from cell lines, cells were first lifted off plates, washed with 1X PBS, and pelleted by centrifugation. These pellets were then lysed and RNA extracted using the AllPrep DNA/RNA Mini Kit (Qiagen, MD). RNA Seq analysis was performed by the in-house Genomics Core Facility at The Cleveland Clinic. Briefly, the total RNA samples were enriched for mRNAs, followed by library preparation and fragmentation using the Illumina TruSeq Kit (Illumina, CA). Paired-end 100 bp sequencing reads were generated using the Illumina NovaSeq 6000 machine (Illumina, CA). RNA-Seq read pre-processing was done using *fastp* with low complexity filters set and trimmed from both 3' and 5' ends.[36] Reads were then aligned to human genome gencode v40 using STAR aligner in gene quantification mode with 2 pass enabled.[37] Differential expression was performed using R package *edgeR.*[38] Pathway enrichment

was completed using Hallmark Gene Set from MsigDB and p-values were calculated via hypergeometric distribution.[39]

Graphs and statistical analyses.

Statistical analyses for TCGA clinical data were performed using R 4.2.1 and R Studio 2021.09.1.[40] For all analyses in R, data in the form of Excel tables were read into R using the readxl package.[41] For Kaplan-Meier analysis, Cox proportional hazards statistical analysis was performed and the results are those quoted. Survival analyses were performed using R package survival[42,43]and survival graphs were generated with survminer.[44] Graphs were generated and statistical analyses were performed for drug radiosensitization studies using the BIGL package.[45] All graphs for clinical data were generated in R using the ggplot2 and RColorBrewer packages.[46,47] Statistical analyses for cell line data were performed using the GraphPad Prism software (Version 8.4.3, GraphPad, CA). Graphs for cell line data were generally made using GraphPad Prism software, except those for Figures 2A, 2B, and 3C, which were generated using the R packages for clinical data above, as well as the ggbeeswarm package.[48] All clinical data summary tables were generated using the gtsummary package.[49] R code for graphs, tables, and statistical analyses are available on GitHub at the following address (www.github.com/petty1284/TP53-and-Endometrial-Cancer).

1. Siegel RL, Miller KD, Fuchs HE, Jemal A. Cancer statistics, 2022. *CA Cancer J Clin*. 2022;72(1):7-33. doi:10.3322/CAAC.21708

2. Sheikh MA, Althouse AD, Freese KE, et al. USA endometrial cancer projections to 2030: should we be concerned? *Future Oncol*. 2014;10(16):2561-2568. doi:10.2217/fon.14.192

3. Kandoth C, Schultz N, Cherniack AD, et al. Integrated genomic characterization of endometrial carcinoma. *Nature*. 2013;497(7447):67-73. doi:nature12113 [pii] 10.1038/nature12113

4. Suarez AA, Felix AS, Cohn DE. Bokhman Redux: Endometrial cancer "types" in the 21st century. *Gynecol Oncol*. 2017;144(2):243-249. doi:10.1016/J.YGYNO.2016.12.010

5. Bosse T, Nout RA, McAlpine JN, et al. Molecular Classification of Grade 3 Endometrioid Endometrial Cancers Identifies Distinct Prognostic Subgroups. *American Journal of Surgical Pathology*. 2018;42(5):561-568. doi:10.1097/PAS.0000000000001020

6. Joehlin-Price A, Van Ziffle J, Hills NK, Ladwig N, Rabban JT, Garg K. Molecularly Classified Uterine FIGO Grade 3 Endometrioid Carcinomas Show Distinctive Clinical Outcomes But Overlapping Morphologic Features. *Am J Surg Pathol*. 2021;45(3):421-429. doi:10.1097/PAS.0000000000001598

7. Murali R, Soslow RA, Weigelt B. Classification of endometrial carcinoma: More than two types. *Lancet Oncol*. 2014;15(7):e268-e278. doi:10.1016/S1470-2045(13)70591-6

8. Van Den Heerik ASVM, Horeweg N, Nout RA, et al. PORTEC-4a: international randomized trial of molecular profile-based adjuvant treatment for women with high-intermediate risk endometrial cancer. *Int J Gynecol Cancer*. 2020;30(12):2002-2007. doi:10.1136/IJGC-2020-001929

9. León-Castillo A, de Boer SM, Powell ME, et al. Molecular Classification of the PORTEC-3 Trial for High-Risk Endometrial Cancer: Impact on Prognosis and Benefit From Adjuvant Therapy. *J Clin Oncol*. 2020;38(29):3388-3397. doi:10.1200/JCO.20.00549

10. Randall ME, Filiaci V, McMeekin DS, et al. Phase III trial: Adjuvant pelvic radiation therapy versus vaginal brachytherapy plus paclitaxel/ carboplatin in high-intermediate and high-risk early stage endometrial cancer. *Journal of Clinical Oncology*. 2019;37(21):1810-1818. doi:10.1200/JCO.18.01575

11. Agapova LS, Ilyinskaya G V., Turovets NA, Ivanov A V., Chumakov PM, Kopnin BP. Chromosome changes caused by alterations of p53 expression. *Mutat Res*. 1996;354(1):129-138. doi:10.1016/0027-5107(96)00062-0

12. Graham NA, Minasyan A, Lomova A, et al. Recurrent patterns of DNA copy number alterations in tumors reflect metabolic selection pressures. *Mol Syst Biol*. 2017;13(2):914. doi:10.15252/MSB.20167159

13. Weiss MB, Vitolo MI, Mohseni M, et al. Deletion of p53 in human mammary epithelial cells causes chromosomal instability and altered therapeutic response. *Oncogene 2010 29:33*. 2010;29(33):4715-4724. doi:10.1038/onc.2010.220

14. Mathias C, Bortoletto S, Centa A, et al. Frequency of the TP53 R337H variant in sporadic breast cancer and its impact on genomic instability. *Sci Rep*. 2020;10(1). doi:10.1038/S41598-020-73282-Y

15. Short NJ, Montalban-Bravo G, Hwang H, et al. Prognostic and therapeutic impacts of mutant TP53 variant allelic frequency in newly diagnosed acute myeloid leukemia. *Blood Adv*. 2020;4(22):5681-5689. doi:10.1182/bloodadvances.2020003120

16. Fei P, El-Deiry WS. P53 and radiation responses. *Oncogene*. 2003;22(37):5774-5783. doi:10.1038/SJ.ONC.1206677

17. Creutzberg CL, Van Putten WLJ, Koper PCM, et al. Surgery and postoperative radiotherapy versus surgery alone for patients with stage-1 endometrial carcinoma: Multicentre randomised trial. *Lancet*. 2000;355(9213):1404-1411. doi:10.1016/S0140-6736(00)02139-5

18. Keys HM, Roberts JA, Brunetto VL, et al. A phase III trial of surgery with or without adjunctive external pelvic radiation therapy in intermediate risk endometrial adenocarcinoma: A Gynecologic Oncology Group study. *Gynecol Oncol*. 2004;92(3):744-751. doi:10.1016/j.ygyno.2003.11.048

19. Bendifallah S, Canlorbe G, Raimond E, et al. A clue towards improving the European Society of Medical Oncology risk group classification in apparent early stage endometrial cancer? Impact of lymphovascular space invasion. *Br J Cancer*. 2014;110(11):2640-2646. doi:10.1038/bjc.2014.237

20. Montalban-Bravo G, Kanagal-Shamanna R, Benton CB, et al. Genomic context and TP53 allele frequency define clinical outcomes in TP53-mutated myelodysplastic syndromes. *Blood Adv*. 2020;4(3):482. doi:10.1182/BLOODADVANCES.2019001101

21. Jiang L, Ye L, Ma L, et al. Predictive values of mutational variant allele frequency in overall survival and leukemic progression of myelodysplastic syndromes. *J Cancer Res Clin Oncol*. 2022;148(4):845-856. doi:10.1007/S00432-021-03905-Y

22. Belickova M, Vesela J, Jonasova A, et al. TP53 mutation variant allele frequency is a potential predictor for clinical outcome of patients with lower-risk myelodysplastic syndromes. *Oncotarget*. 2016;7(24):36266-36279. doi:10.18632/ONCOTARGET.9200

23. Deng J, Wu X, Ling Y, et al. The prognostic impact of variant allele frequency (VAF) in TP53 mutant patients with MDS: A systematic review and meta-analysis. *Eur J Haematol*. 2020;105(5):524-539. doi:10.1111/EJH.13483

24. Abazeed ME, Adams DJ, Hurov KE, et al. Integrative radiogenomic profiling of squamous cell lung Cancer. *Cancer Res*. Published online 2013. doi:10.1158/0008-5472.CAN-13-1616

25. Michaelis M, Rothweiler F, Barth S, et al. Adaptation of cancer cells from different entities to the MDM2 inhibitor nutlin-3 results in the emergence of p53-mutated multi-drug-resistant cancer cells. Published online 2011. doi:10.1038/cddis.2011.129

26. Pal S, Yadav P, Sainis KB, Shankar BS. TNF-α and IGF-1 differentially modulate ionizing radiation responses of lung cancer cell lines. *Cytokine*. 2018;101:89-98. doi:10.1016/J.CYTO.2016.06.015

27. Sathishkumar S, Dey S, Meigooni AS, et al. The impact of TNF-alpha induction on therapeutic efficacy following high dose spatially fractionated (GRID) radiation. *Technol Cancer Res Treat*. 2002;1(2):141-147. doi:10.1177/153303460200100207

28. Barkett M, Gilmore TD. Control of apoptosis by Rel/NF-kappaB transcription factors. *Oncogene*. 1999;18(49):6910-6924. doi:10.1038/SJ.ONC.1203238

29. Grimm S, Bauer MKA, Baeuerle PA, Schulze-Osthoff K. Bcl-2 down-regulates the activity of transcription factor NF-kappaB induced upon apoptosis. *J Cell Biol*. 1996;134(1):13-23. doi:10.1083/JCB.134.1.13

30. Kimura K, Gelmann EP. Propapoptotic effects of NF-κB in LNCaP prostate cancer cells lead to serine protease activation. *Cell Death & Differentiation 2002 9:9*. 2002;9(9):972-980. doi:10.1038/sj.cdd.4401049

31. Schneider G, Krämer OH. NFκB/p53 crosstalk—a promising new therapeutic target. *Biochimica et Biophysica Acta (BBA) - Reviews on Cancer*. 2011;1815(1):90-103. doi:10.1016/J.BBCAN.2010.10.003

32. Gao J, Aksoy BA, Dogrusoz U, et al. Integrative analysis of complex cancer genomics and clinical profiles using the cBioPortal. *Sci Signal*. 2013;6(269). doi:10.1126/SCISIGNAL.2004088

33. Cerami E, Gao J, Dogrusoz U, et al. The cBio Cancer Genomics Portal: An Open Platform for Exploring Multidimensional Cancer Genomics Data. *Cancer Discov*. 2012;2(5):401-404. doi:10.1158/2159-8290.CD-12-0095

34. Shalem O, Sanjana NE, Hartenian E, et al. Genome-scale CRISPR-Cas9 knockout screening in human cells. *Science (1979)*. 2014;343(6166):84-87. doi:10.1126/science.1247005

35. Sanjana NE, Shalem O, Zhang F. Improved vectors and genome-wide libraries for CRISPR screening. *Nat Methods*. 2014;11(8):783-784. doi:10.1038/nmeth.3047

36. Chen S, Zhou Y, Chen Y, Gu J. Fastp: An ultra-fast all-in-one FASTQ preprocessor. In: *Bioinformatics*. Vol 34. ; 2018. doi:10.1093/bioinformatics/bty560

37. Dobin A, Davis CA, Schlesinger F, et al. STAR: Ultrafast universal RNA-seq aligner. *Bioinformatics*. 2013;29(1). doi:10.1093/bioinformatics/bts635

38. Chen Y, Lun ATL, Smyth GK. Differential Expression Analysis of Complex RNA-seq Experiments Using edgeR. In: *Statistical Analysis of Next Generation Sequencing Data*. ; 2014. doi:10.1007/978-3-319-07212-8_3

39. Liberzon A, Subramanian A, Pinchback R, Thorvaldsdóttir H, Tamayo P, Mesirov JP. Molecular signatures database (MSigDB) 3.0. *Bioinformatics*. 2011;27(12). doi:10.1093/bioinformatics/btr260

40. R Core Team. R: A Language and Environment for Statistical Computing. Published online 2022.

41. Wickham H BJ. Read Excel Files [R package readxl version 1.4.1]. Published online August 17, 2022.

42. Therneau TM. A Package for Survival Analysis in R. Published online 2022.

43. Terry M. Therneau, Patricia M. Grambsch. *Modeling Survival Data: Extending the Cox Model*. Springer; 2000.

44. Kassambara A, Kosinski M, Biecek P. survminer: Drawing Survival Curves using “ggplot2.” Published online 2021.

45. Turner H, Tourny A, Thas O, Nazarov M, Bagdziunas R, Hawinkel S. BIGL: Biochemically Intuitive Generalized Loewe Model. Published online 2022.

46. Wickham H. *Ggplot2: Elegant Graphics for Data Analysis*. Springer-Verlag New York; 2016.

47. Neuwirth E. RColorBrewer: ColorBrewer Palettes. Published online 2022.

48. Clarke E, Sherrill-Mix S. ggbeeswarm: Categorical Scatter (Violin Point) Plots. Published online 2017.

49. Sjoberg DD, Whiting K, Curry M, Lavery JA, Larmarange J. Reproducible Summary Tables with the gtsummary Package. *R J*. 2021;13(1):570-580. doi:10.32614/RJ-2021-053

Figure 1. TP53 Variant Allelic Frequency Is Clinically Relevant in Endometrial Cancer

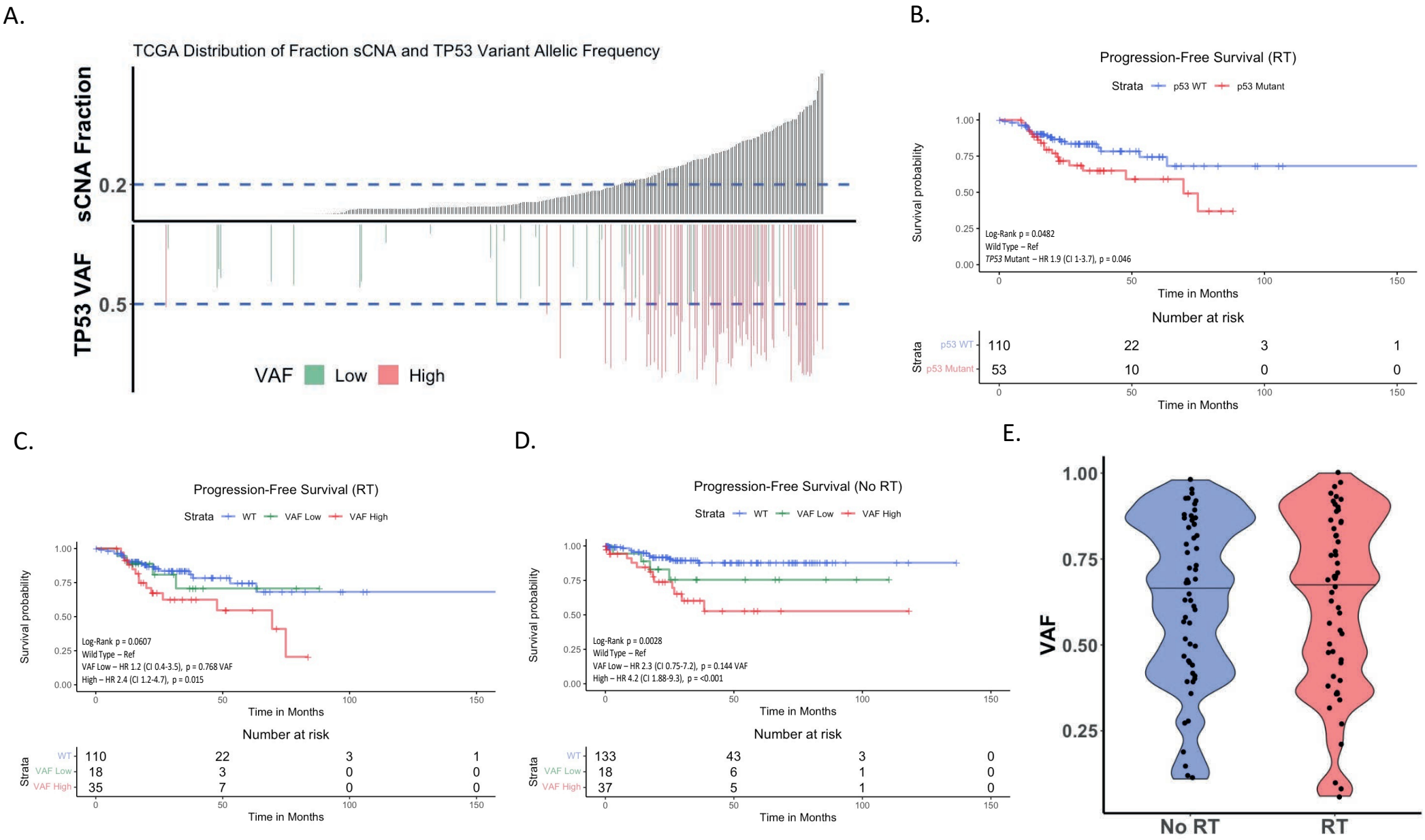

Figure 1. TP53 Variant Allelic Frequency Is Clinically Relevant in Endometrial Cancer - A) This plot represents available EC patients in cbioportal with somatic copy number alteration (sCNA) burden and TP53 data available. The dashed line at 0.2 defines the cutoff for copy-number high used in TCGA. As noted, the frequency of TP53 mutations increases with increasing sCNA. While the majority of TP53 mutations have a high variant allelic frequency (VAF), there remain patients with <50% allelic frequency throughout the entire population. **B-D)** Kaplan-Meier plots and Cox-regression for progression free survival (PFS) stratified by TP53 status **(B)** and TP53 VAF **(C-D)**. As noted in subfigure B, patients with TP53 mutation had worse PFS compared to wild-type patients when treated with RT. When stratified by VAF (**C),** patients with a high VAF had a worse PFS compared to low VAF and wild-type patients. We observed the same in non-RT patients **(D)**, albeit the difference in risk of progression based on hazard ratio was more notable between low VAF and wild-type. **E)** Violin plot representing the overall distribution of TP53 VAF in both treatment groups, highlighting that current treatment patterns do not take VAF into consideration.

Table 1. Stratification of *TP53* mutant patients based on VAF highlights other associated genomic markers.

Characteristic	P53 Variant Allele Frequency		
	High, N = 72[1]	**Low**, N = 36[1]	**p-value**[2]
Age at Diagnosis	69.00 (8.88)	64.00 (10.64)	0.057
Total Mutation Count	60.00 (42.28)	176.50 (2,837.31)	<0.001
Fraction Genome Altered	0.43 (0.18)	0.15 (0.19)	<0.001
TCGA Cluster			<0.001
UCEC_CN_HIGH	67 / 69 (97%)	16 / 36 (44%)	
UCEC_CN_LOW	1 / 69 (1.4%)	4 / 36 (11%)	
UCEC_MSI	1 / 69 (1.4%)	13 / 36 (36%)	
UCEC_POLE	0 / 69 (0%)	3 / 36 (8.3%)	
FIGO Stage			>0.9
I	37 / 72 (51%)	20 / 36 (56%)	
II	10 / 72 (14%)	4 / 36 (11%)	
III	25 / 72 (35%)	12 / 36 (33%)	
Histologic Grade			0.4
1	0 / 72 (0%)	1 / 36 (2.8%)	
2	7 / 72 (9.7%)	4 / 36 (11%)	
3	65 / 72 (90%)	31 / 36 (86%)	
Radiation Therapy	35 / 72 (49%)	18 / 36 (50%)	0.9

[1] Median (SD); n / N (%)

[2] Wilcoxon rank sum test; Fisher's exact test; Pearson's Chi-squared test

Table 1. Stratification of TP53 mutant patients based on VAF highlights other associated genomic markers. Demographics table of patients with TP53 alterations stratified by their variant allelic frequency. High is defined as >50% and low is defined as <50%. As noted, patients with a low VAF were more likely to have higher mutational counts, lower copy-number alterations, and less likely to be classified into the "serous-like" (UCEC_CN-HIGH) TCGA cluster. When taken as an entire group, the "serous-like" cluster had 105 patients, with 16 (15%) falling into the low VAF classification. No differences in clinical stage, histologic grade, or receipt of adjuvant radiation (RT) therapy was noted.

Figure 2. *TP53* Status and VAF are Associated with Radiation Resistance in EC Cell Lines

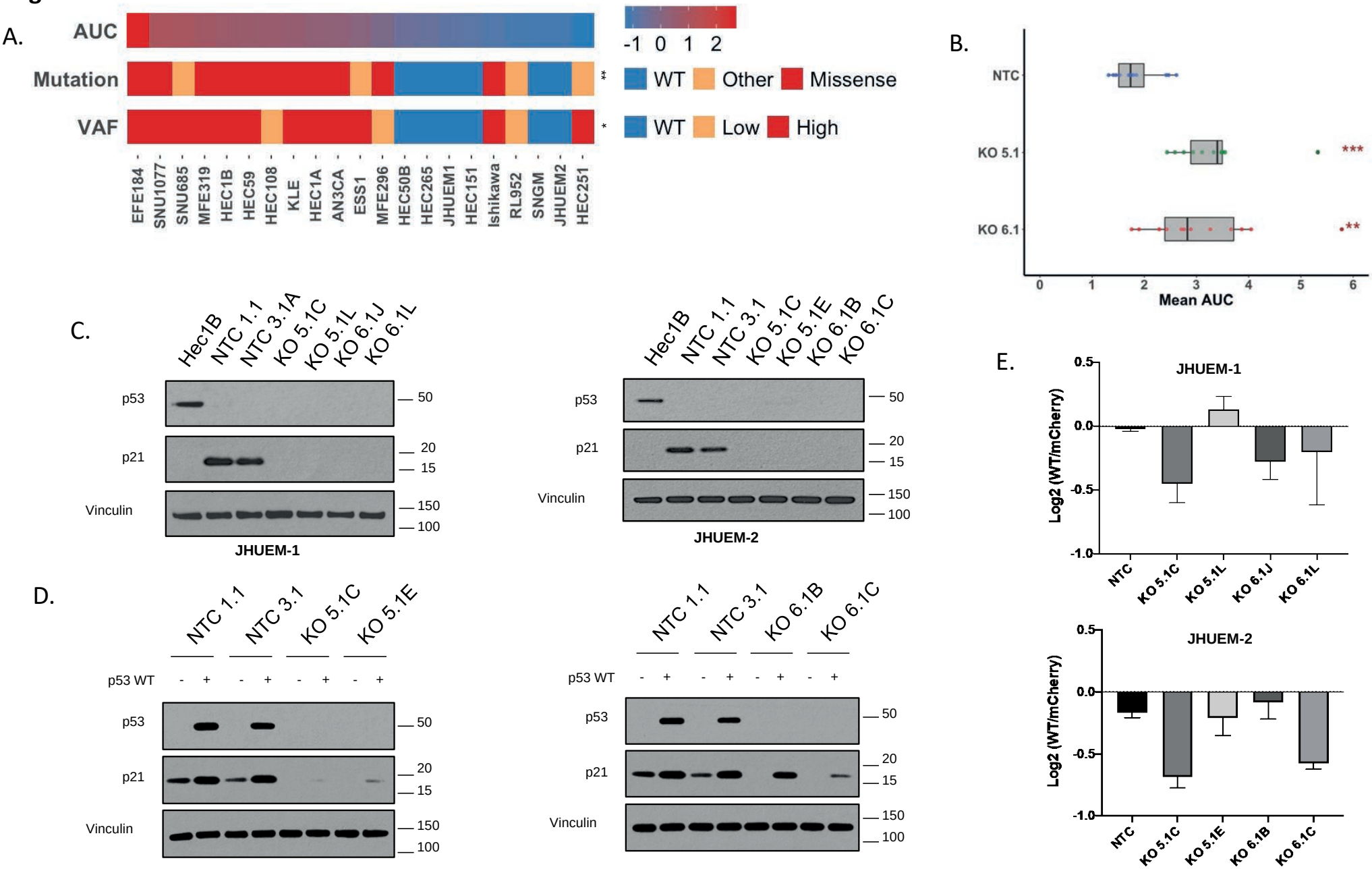

Figure 2. *TP53* Status and AF are Associated with Radiation Resistance in EC Cell Lines – A) Heat-map depicting 21 EC cell lines organized by decreasing radiation resistance (left to right) as quantified by area under the curve (AUC). The cell lines' TP53 mutational status and VAF are depicted in the bars below, denoting the significant associations between AUC and *TP53* mutation status ($p = 0.004$) or VAF ($p = 0.01$), respectively. A linear regression model was fitted to assess for the correlation between mutation and AUC (Likelihood Ratio = 11.12 and P= 0.0038) as well as VAF and AUC (Likelihood Ratio = 9.42 and P= 0.009). **B)** Box-whisker plot depicting the increase in radiation AUC noted with two different CRISPR/Cas9 guide-RNA (gRNA) sequences for TP53 compared to the non-targeting control (NTC). Kruskal-Wallis test with Dunn's Multiple Comparisons Test was performed with $p< 0.001$ for NTC vs KO 5.1, $p = 0.0016$ for NTC vs KO 6.1. **C)** Western-blot analysis of two monoclonal isolates from each gRNA and NTC reveals loss of p21 signaling with knock-out of TP53. Hec1B is our positive control for p53. **D-E)** Complementation with wild-type TP53 re-establishes p21 signaling and radiation sensitivity in knock-out clones. For subfigure E and JHUEM2 ,one- way ANOVA test with Dunnett's Multiple Comparisons test was performed with $p = 0.0051$ for KO 5.1C vs NTC, $p = 0.0199$ for KO 6.1C vs NTC.

Figure 3. Gain-of-Function/Dominant-Negative Alleles of *TP53* Impact p21 Signaling, Radiation Response and apoptosis

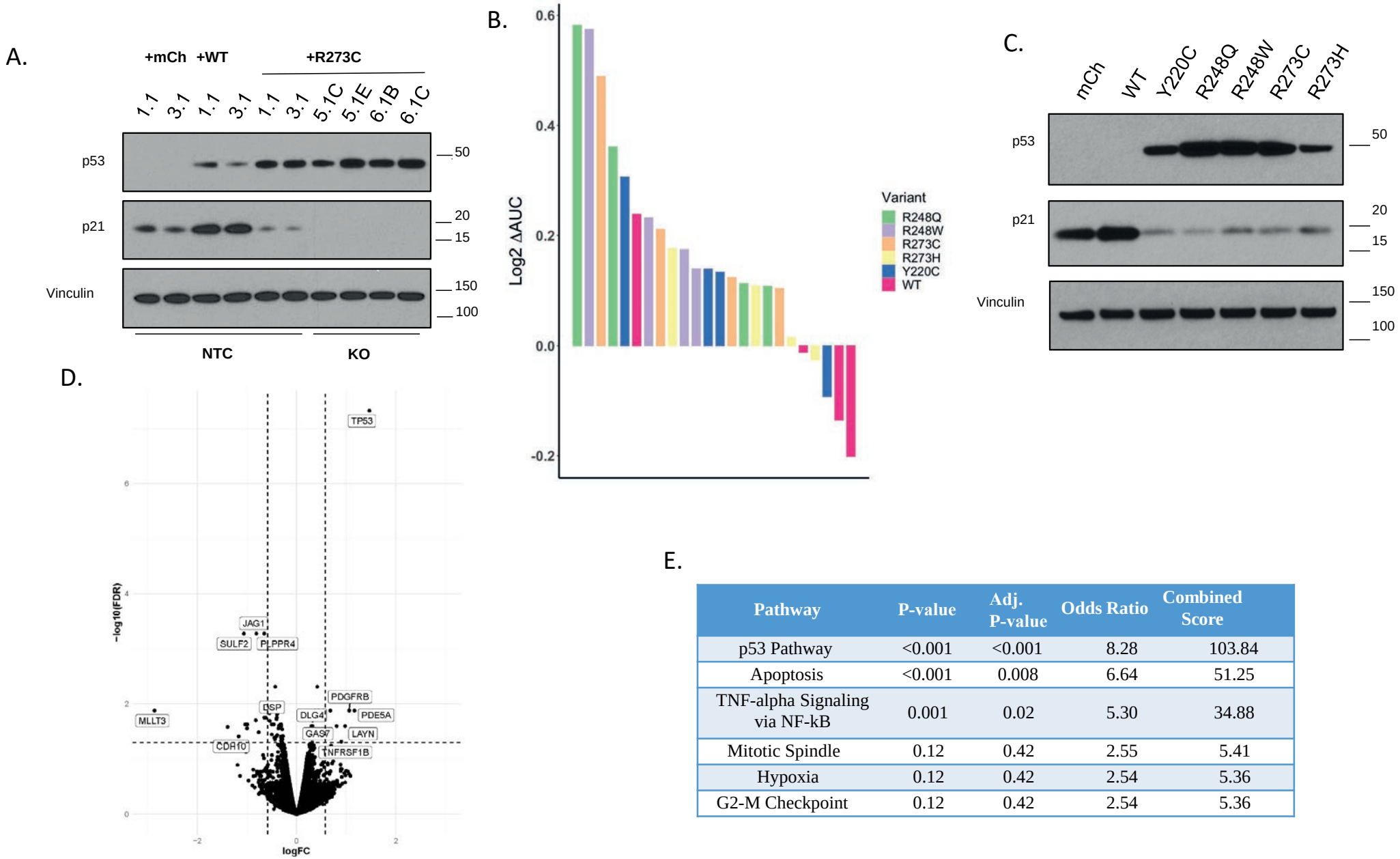

Pathway	P-value	Adj. P-value	Odds Ratio	Combined Score
p53 Pathway	<0.001	<0.001	8.28	103.84
Apoptosis	<0.001	0.008	6.64	51.25
TNF-alpha Signaling via NF-kB	0.001	0.02	5.30	34.88
Mitotic Spindle	0.12	0.42	2.55	5.41
Hypoxia	0.12	0.42	2.54	5.36
G2-M Checkpoint	0.12	0.42	2.54	5.36

Figure 3. Gain-of-Function/Dominant-Negative Alleles of TP53 Impact p21 Signaling, Radiation Response, and Apoptotic Pathways – **A)** Western-blot analysis of JHUEM-2 non-targeting control [NTC] isolates (1.1 and 3.1) with the addition of mcherry (control), wild-type TP53 (over-expression), and the addition of the R273C allele (co-expression with wild-type). A decrease in p21 signaling after introduction of the R273C allele is noted in the NTC isolated, despite parental/wild-type TP53 alleles. In the knockout isolates (5.1C/E and 6.1B/C) there is no p21 signaling observed with the mutant allele alone. **B)** Waterfall plot depicting the overall effect on AUC after introduction of a variant allele (or wild-type) across 4 different mono-clonal NTC isolates. As noted, introduction of variant alleles led to an increase in radiation resistance from baseline despite the presence of a wild-type allele. **C)** Western-blot analysis demonstrating decrease in p21 signaling with each analyzed GOF/DN TP53 variant. **D)** Volcano plot analysis of an the NTC isolates with R273C co-expression, compared to the NTC alone (wild-type) 24hr after 2Gy irradiation. An increase in the expression of TP53 in our wt/R273C isolate confirms increased expression of p53, with a decrease in the expression of genes associated with apoptosis and TNF-alpha signaling **(E).**

Figure 4. MDM2 Inhibition with Nutlin-3 and AMG-232 as a Cytotoxic Strategy

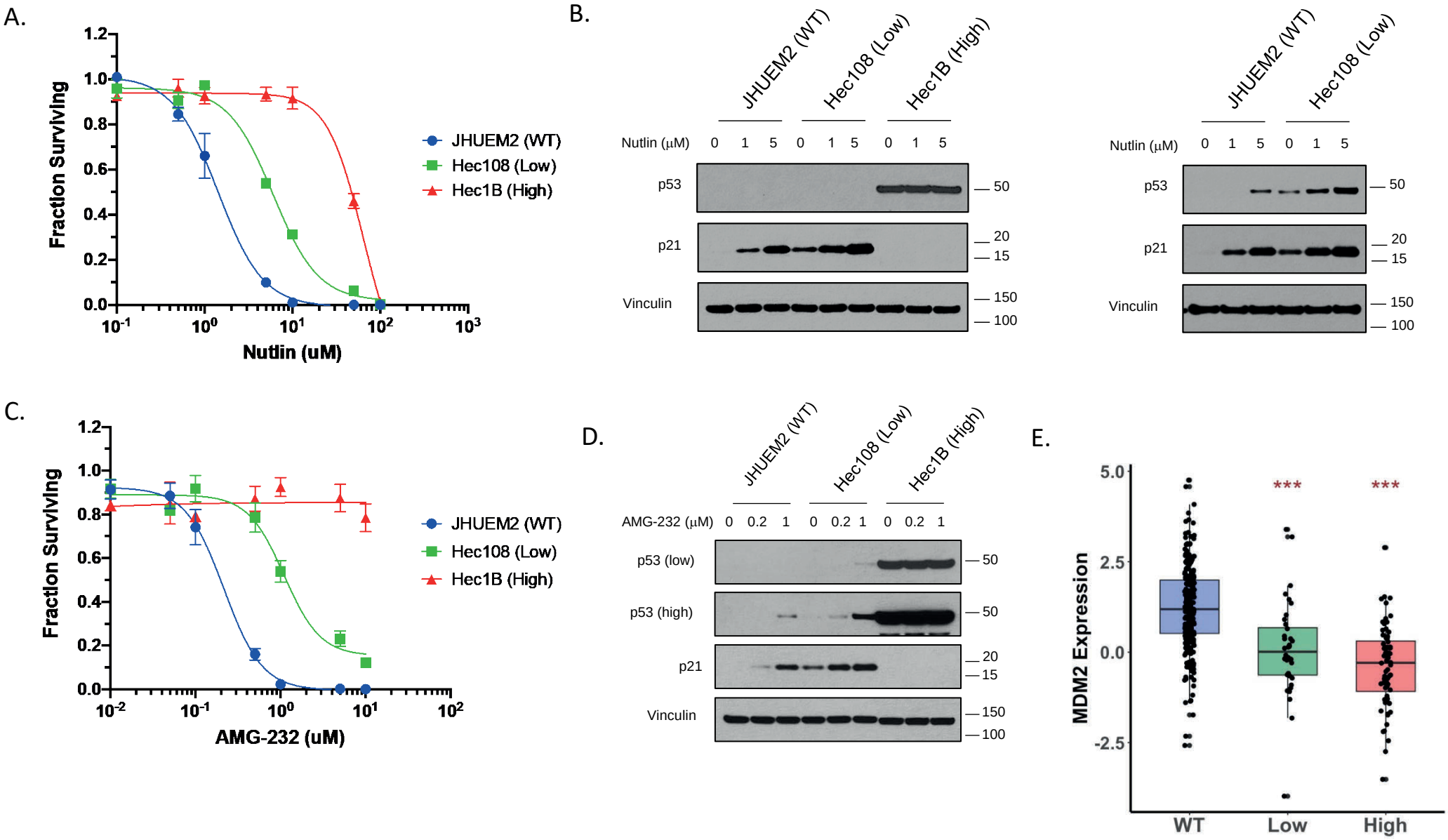

Figure 4. MDM2 Inhibition with Nutlin-3 and AMG-232 as a Cytotoxic Strategy. A, C) – Drug response curve of EC cell lines representing three different VAF populations – JHUEM2 (wild-type), Hec108 (low-VAF), and Hec1B (high-VAF). Nutlin-3 **(A)** and AMG-232 **(C)** both demonstrate significant effects on cell viability in JHUEM2 and Hec 108. Hec1B was resistant to treatment with either drug. **B, D)** Western-blot analysis of all three cell lines demonstrate an increase in p53/p21 with increasing concentrations of either drug. **E)** Box-whisker plot of MDM2 expression across TCGA patients demonstrate that MDM2 expression decreases with increasing VAF, but there remains a significant portion of low-VAF patients with mRNA expression that could be targeted via Nutlin-3/AMG-232. For subfigure E, one-way ANOVA with Tukey's Multiple Comparisons Test was conducted to analyze relative expression compared to the WT group. $p < 0.001$ for Low vs WT ; $p < 0.001$ for High vs WT.

Figure 5. MDM2 Inhibition Is Synergistic with Radiotherapy in EC with Wild-Type *TP53*

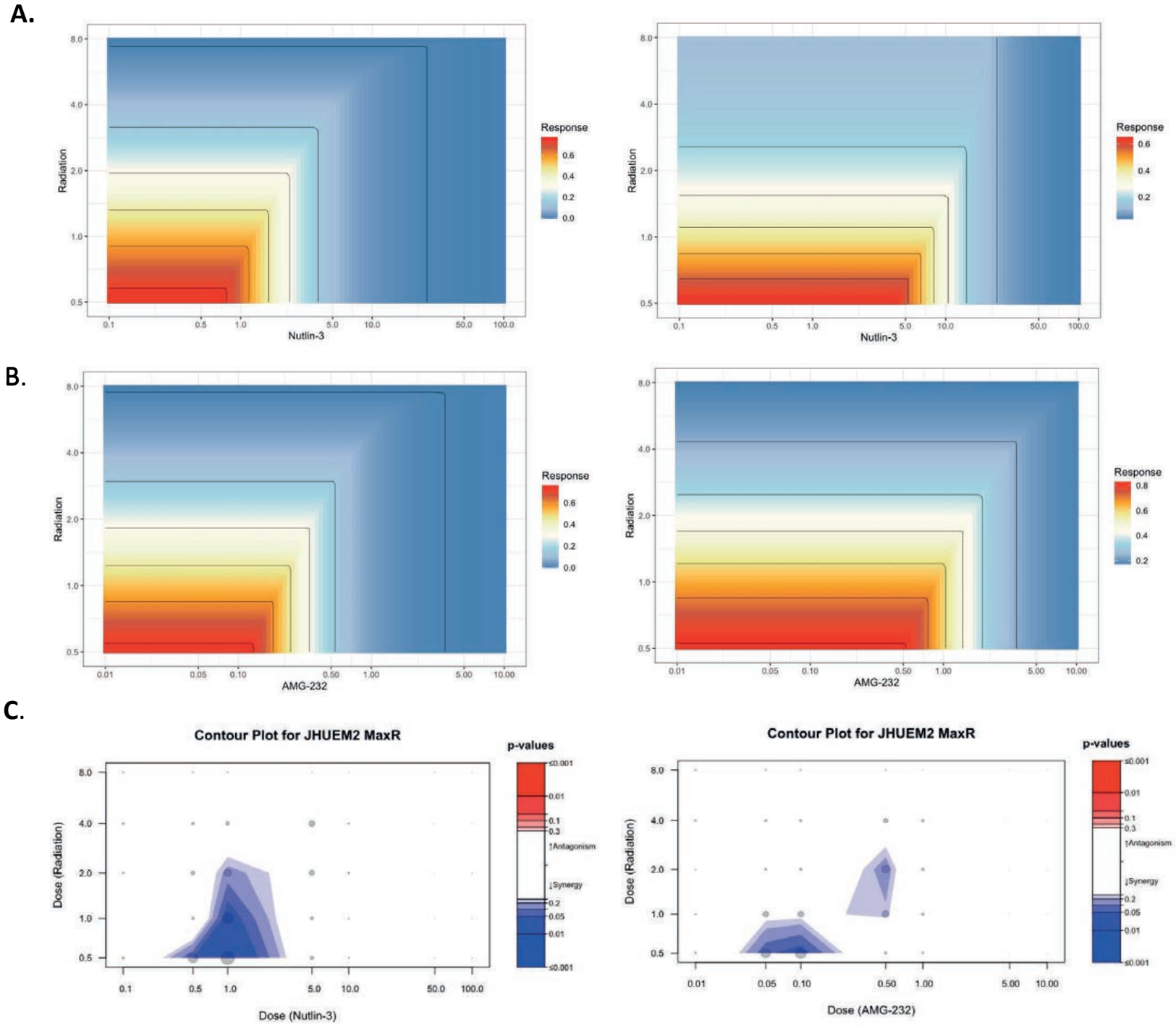

Figure 5. MDM2 Inhibition Is Synergistic (or Additive) with Radiotherapy Dependent on TP53 Status – A-B) Isobolograms for Nutlin-3 **(A)** and AMG-232 **(B)** in two EC cell lines - JHUEM2 (left) and Hec108 (right) - treated with gamma irradiation. As depicted, increasing drug dosage is the x-axis and increasing radiation dose is the y-axis. A robust effect on Nutlin-3 and AMG-232 is achieved at low drug concentrations and low RT doses for both the wild-type (JHUEM2) and low VAF (Hec108) cell line. **C)** Contour plots quantitatively demonstrate the synergistic effect of Nutlin-3 in JHUEM2 (left), as well as with AMG-232 in JHUEM2 (right) and Hec108(supp Fig 5). The remaining interactions were classified as additive. Synergy was quantified by comparing actual values to those predicted by fitting the Highest Single Agent (HSA) model to the data.